Bayesian inference of solid-liquid interfacial properties out of equilibrium

Munekazu Ohno,[1,*] Yukimi Oka,[2] Shinji Sakane,[3] Yasushi Shibuta,[4] and Tomohiro Takaki[5]
[1]*Faculty of Engineering, Hokkaido University, Kita 13 Nishi 8, Kita-ku, Sapporo, Hokkaido 060-8628, Japan*
[2]*Graduate School of Engineering, Hokkaido University, Kita 13 Nishi 8, Kita-ku, Sapporo, Hokkaido 060-8628, Japan*
[3]*Graduate School of Science and Technology, Kyoto Institute of Technology, Matsugasaki, Sakyo-ku, Kyoto 606-8585, Japan*
[4]*Department of Materials Engineering, The University of Tokyo, 7-3-1 Hongo, Bunkyo-ku, Tokyo 113-8656, Japan*
[5]*Faculty of Mechanical Engineering, Kyoto Institute of Technology, Matsugasaki, Sakyo-ku, Kyoto 606-8585, Japan*

(Received 10 January 2020; accepted 27 April 2020; published 18 May 2020)

Solid-liquid interfacial properties out of equilibrium provide the essential information required for understanding and controlling solidification microstructures in metallic materials. However, few studies have attempted to reveal all interfacial properties out of equilibrium in detail. The present study proposes an approach for simultaneously estimating all interfacial properties in a pure metal below the melting point on the basis of the Bayesian inference theory. The solid-liquid interfacial energy, interfacial mobility, and anisotropy parameters in pure Fe are estimated by combining molecular dynamics simulation with phase-field simulation using an ensemble Kalman filter, which is a data assimilation technique. Furthermore, the temperature dependences of all interfacial parameters are computed and discussed. In summary, the proposed multiscale approach integrates atomistic and microstructural simulations within the framework of data science and it has considerable potential for a wide variety of applications in materials engineering.

DOI: 10.1103/PhysRevE.101.052121

I. INTRODUCTION

The evolution and devolution processes of solidification microstructures in metallic materials originate from the interface dynamics, which are controlled by the solid-liquid interfacial properties, such as the interfacial energy and mobility as well as their dependences on the crystallographic orientation of the solid, i.e., their anisotropies [1]. As solidification microstructures are products of nonequilibrium processes, prediction and control of the microstructural processes essentially require the knowledge of solid-liquid interfacial properties out of equilibrium.

Accurate determination of the physical parameters associated with microstructural processes is one of the most important issues to be addressed for the advancement of techniques for controlling microstructures [2]. Several experimental methods have been developed for determining solid-liquid interfacial properties [3–5]. Moreover, solid-liquid interfacial properties have been extensively investigated in theoretical studies [6–8] and numerical studies based on the classical density-functional theory [9–11] and the phase-field crystal theory [12]. Currently, atomistic simulation, such as molecular dynamics (MD) simulation, is considered as a method of choice for determining solid-liquid interfacial properties with high accuracy [13,14]. The capillary fluctuation method (CFM) [15] and cleaving technique (CT) [16] were developed for computing the solid-liquid interfacial energy σ_0 and its anisotropy parameter ε_c, which will be defined later in detail, via MD simulation. They have been successfully applied to several metallic materials [14]. Furthermore, the interfacial mobility μ_0 and its anisotropy parameter ε_k can be evaluated, for instance, by measuring the solid-liquid interfacial velocity in an undercooled melt via MD simulation [17]. These approaches have contributed toward widening the application range of microstructure simulation, such as phase-field simulation [1,13,14]. However, determining all interfacial parameters is not a trivial task because it requires elaborate analyses with a combination of different types of MD simulation. Accordingly, not all interfacial parameters have been computed for many metallic materials. In this regard, it is desirable to develop an efficient approach for clarifying all the properties simultaneously and accurately from a single MD simulation, which is tackled in this work.

Solidification is a nonequilibrium phenomenon. As solidification in pure metals takes place in an undercooled melt, simulation of the solidification microstructures in pure metals requires the interfacial parameters to be determined below the melting point T_m. However, for instance, the CFM and CT have so far been applied only to flat and static interfaces in equilibrium and questions about σ_0 and ε_c out of equilibrium remain to be answered. Early theoretical and numerical studies implicitly or explicitly indicated that σ_0 monotonically increases with the temperature [6–9,14,18,19]. In other words, it exhibits a positive temperature dependence. However, some theoretical studies have shown that the temperature dependence of σ_0 is not monotonic [20,21]. More specifically, as the temperature increases, σ_0 increases in low-temperature regions and then decreases near T_m. Such a negative temperature dependence near the transition temperature has often been found in studies of other interfacial energies, such as the surface tensions of pure liquid and solid metals [22,23] and antiphase boundary energies in ordered systems [24,25]. Moreover, a recent study based on metadynamics MD

*Corresponding author:mohno@eng.hokudai.ac.jp

simulation with the Lennard-Jones potential demonstrated the possibility of the negative temperature dependence of σ_0 [26]. Hence, further investigation is required for clarifying the temperature dependence of σ_0. In addition, simulation of solidification microstructures at undercooling temperatures requires the knowledge of the temperature dependences of ε_c, μ_0, and ε_k as well as σ_0.

The rapid development of high-performance computing techniques has made it possible to scale up MD simulation to the level of small microstructures [27–31]. Currently, we can directly compare the time evolution processes of solidification microstructures described by MD and a continuum model such as the phase-field model [31]. Such overlap of spatial and temporal scales of both methods allows simultaneous use of information from different scales in collaboration with recent techniques from data science. Here we present an approach for computing all the parameters of solid-liquid interfaces out of equilibrium on the basis of an ensemble-based Bayesian inference approach, i.e., data assimilation technique [32–34] combined with MD and phase-field simulations. The data assimilation offers a technique for combining observation data with a simulation model to estimate the model parameters and/or states of the system. Feasibility studies on the parameter estimation of phase-field models for solid-state transformations on the basis of data assimilation have recently been conducted within the framework of the so-called twin experiments, i.e., testing of estimation with the use of hypothetical data [35,36]. In this study, we demonstrate that all the interfacial parameters for solidification in a pure metal out of equilibrium can be simultaneously estimated on the basis of an ensemble Kalman filter (EnKF) [34], where the simulation model is the phase-field model and the observation data are microstructural data obtained by the MD simulation reported in our previous study [27]. Further, we investigate the temperature dependences of all the interfacial parameters.

The remainder of this paper is organized as follows. Section II introduces the interfacial parameters for isothermal solidification in a pure metal, which is the main focus of this study. Sections III, IV, and V describe the phase-field model, MD simulation, and EnKF, respectively. Section VI discusses the parameter estimation results and temperature dependences of all the interfacial parameters. A summary is provided in Sec. VII.

II. INTERFACIAL PARAMETERS FOR ISOTHERMAL SOLIDIFICATION IN A PURE METAL

In isothermal solidification of a pure metal, the interface dynamics is described by the Gibbs-Thomson equation [37,38]

$$v_n = \mu(\mathbf{n})\left[\Delta G_{\mathrm{driv}} - \sum_{i=1,2}\left(\sigma(\mathbf{n}) + \frac{\partial^2\sigma}{\partial\theta_i^2}\right)\kappa_i\right], \tag{1}$$

where v_n is the interfacial velocity in the direction normal to the interface, $\mu(\mathbf{n})$ is the interfacial mobility with the unit vector normal to the interface $\mathbf{n}$, ΔG_{driv} is the driving force of solidification, $\sigma(\mathbf{n})$ is the solid-liquid interfacial energy, θ_i is the angle between $\mathbf{n}$ and the direction of principal curvature of the interface specified by i, and κ_i is the principal curvature of the interface. When the average values of $\mu(\mathbf{n})$ and $\sigma(\mathbf{n})$ are denoted by μ_0 and σ_0, respectively, $\mu(\mathbf{n})$ and $\sigma(\mathbf{n})$ can be described as $\mu(\mathbf{n}) = \mu_0 a_k(\mathbf{n})$ and $\sigma(\mathbf{n}) = \sigma_0 a_c(\mathbf{n})$ with anisotropy functions $\alpha_k(\mathbf{n})$ and $\alpha_c(\mathbf{n})$, respectively [37–39].

In this study, we focus on the (quasi-)two-dimensional (2D) growth of a solid in an undercooled melt of pure Fe, which was investigated in the previous MD simulation [27]. The anisotropy functions are given as $a_c(\mathbf{n}) = 1 + \varepsilon_c\cos(4\theta)$ and $a_k(\mathbf{n}) = 1 - e_k\cos(4\theta)$ [39], where ε_c and ε_k are the anisotropy parameters of the interfacial energy and mobility, respectively, and θ is the angle between the interface normal and $\langle 100\rangle$ of the crystal. Furthermore, the driving force ΔG_{driv} can be approximated as $\Delta G_{\mathrm{driv}} = \Delta H\Delta T/T_m$, where ΔH is the latent heat and ΔT is the degree of undercooling. Then Eq. (1) can be rewritten as

$$u_{\mathrm{int}} = \frac{T_m c_p}{\Delta H^2}\sigma_0[1 - 15\epsilon_c\cos(4\theta)]\kappa + \beta_0[1 - \epsilon_k\cos(4\theta)]v_n + \zeta, \tag{2}$$

where u_{int} is the dimensionless undercooling at the interface, defined as $u_{\mathrm{int}} = \Delta T/(\Delta H/c_p)$ with specific heat c_p, and β_0 is the kinetic coefficient defined as $\beta_0 = T_m c_p/\mu_0\Delta H^2$. Here the noise term ζ is added to describe the fluctuation in the interface dynamics.

The interfacial properties in this problem can be completely characterized by four parameters: σ_0, ε_c, β_0, and ε_k. In Eq. (2), bulk quantities such as T_m, c_p, and ΔH can be easily obtained via experimentation and/or simulation, and these data are generally available in the literature. However, it is rather rare that all four interfacial parameters are available. In this study, these four parameters at a given temperature are estimated from a single MD simulation.

III. PHASE-FIELD MODEL

In the phase-field model, the microstructure is characterized by an order parameter called the phase-field ϕ, which takes a value of $+1$ for a solid and -1 for a liquid; ϕ continuously changes from $+1$ to -1 inside the solid-liquid interface. Thus, the interface has a thickness and it is called the diffuse interface. In this model, isothermal solidification in a pure metal can be described by the phase-field equation [39]

$$\tau(\mathbf{n})\frac{\partial\phi}{\partial t} = \nabla[W(\mathbf{n})^2\nabla\phi] + \sum_{i=x,y}\partial_i\left(|\nabla\phi|^2 W(\mathbf{n})\frac{\partial W(\mathbf{n})}{\partial(\partial_i\phi)}\right) + \phi - \phi^3 - \lambda(1-\phi^2)^2 u_{\mathrm{int}} + \tau(\mathbf{n})\xi, \tag{3}$$

where

$$W(\mathbf{n}) = W_0 a_c(\mathbf{n}), \tag{4}$$

$$a_c(\mathbf{n}) = (1 - 3\epsilon_c)\left(1 + \frac{4\epsilon_c}{1 - 3\epsilon_c}\left(n_x^4 + n_y^4\right)\right), \tag{5}$$

$$\tau(\mathbf{n}) = \frac{1}{a_1^2}\frac{W_0^2}{d_0}\beta_0 a_c(\mathbf{n})a_k(\mathbf{n}), \tag{6}$$

$$a_k(\mathbf{n}) = (1 + 3\epsilon_k)\left(1 - \frac{4\epsilon_k}{1 + 3\epsilon_k}\left(n_x^4 + n_y^4\right)\right). \tag{7}$$

Here W_0 is the interface thickness, λ is the coupling constant given by $\lambda = a_1 W_0/d_0$, with $a_1 = 5\sqrt{2}/8$ and d_0 the capillary length defined as $d_0 = \sigma_0(T_m c_p/\Delta H^2)$, $\mathbf{n}$ is the unit vector normal to the interface, and $n_x^4 + n_y^4$ is given by $n_x^4 + n_y^4 = [(\partial\phi/\partial x)^4 + (\partial\phi/\partial y)^4]/|\nabla\phi|^4$. Further, ξ is the noise term that represents the fluctuation of the interface dynamics and it obeys the Gaussian noise distribution whose variance is given by the fluctuation-dissipation theorem as [40,41]

$$\langle \xi(\boldsymbol{r}_i, t_j)\xi(\boldsymbol{r}_k, t_l)\rangle = \frac{2F_\phi}{\Delta t\,\Delta x^2}\delta_{ik}\delta_{jl}, \tag{8}$$

where ΔT is the time step, Δx is the grid spacing in the simulation, δ_{ik} is the Kronecker delta function, and F_ϕ is given by

$$F_\phi = a_R J\lambda \frac{k_B T_m^2 c_p}{\Delta H^2 W_0^2}, \tag{9}$$

where k_B is the Boltzmann constant and $J = 16/15$. Although a_R must be unity, it is varied in our analysis to control the system noise in the EnKF, as explained later. To avoid unstable calculations due to the large contribution of the noise term, the upper and lower limits of ϕ are set to $+1$ and -1, respectively, in the phase-field simulation. Note that Eq. (3) exactly reproduces the Gibbs-Thomson effect given by Eq. (2).

Equation (3) is discretized using a second-order finite-difference scheme with the grid spacing Δx and it is solved using a first-order Euler scheme. As described later, the previous MD simulation [27] was conducted in a quasi-2D system with a size of $53.4 \times 53.4 \times 4.3\,\mathrm{nm}^3$. In the preliminary investigation, we carried out the twin experiments on the basis of 3D phase-field simulation for the quasi-2D system and 2D phase-field simulation to observe the effects of the dimension on the parameter estimation accuracy. Here the twin experiments are conducted to evaluate the accuracy of parameter estimation [32–36]. It is a test of the parameter estimation in which the observation data are not actual MD data, but hypothetical data obtained from phase-field simulation with the use of prescribed (assumed) values of the interfacial parameters in the present case. The twin experiments indicated that there is no significant difference between the estimation accuracies of the 3D and 2D simulations. Therefore, we focus on only 2D phase-field simulation in this study. Furthermore, we checked the effect of the grid spacing Δx on the estimation accuracy by carrying out the simulations with 64^2, 128^2, 256^2, and 512^2 grid points. In view of the trade-off between accuracy and computational cost, the number of grid points is set to 128^2 in all the phase-field simulations described in this paper. The interface thickness is given by $W_0 = 1.5\Delta x$.

The previous MD simulation [27] was carried out using the Finnis-Sinclair (FS) potential [42], which is one of the representative potentials for bcc metals. In this study, accordingly, the bulk quantities ΔH, T_m, and c_p are set to values obtained via MD simulation with the FS potential, i.e., $\Delta H = 2.147 \times 10^9\,\mathrm{J/m^3}$ [17], $T_m = 2400\,\mathrm{K}$ [17], and $c_p = 3.685 \times 10^6\,\mathrm{J/(m^3\,K)}$, which was obtained in the present MD simulation. Then, except for the interfacial parameters, the only remaining input parameter in Eq. (3) is u_{int}, which is determined from the results of the previous MD simulation [27], as described in the next section.

IV. MD SIMULATION FOR ISOTHERMAL GROWTH OF A BCC CRYSTAL

Recent high-performance computing techniques, especially those involving a graphics processing unit (GPU), allow large-scale MD simulation of solidification microstructures [27–31]. Solidification in pure Fe was investigated via MD simulation, where a single solid grows in the undercooled melt [27]. This process is basically dominated by the Gibbs-Thomson relation given by Eqs. (2) and (3). In this study, the results of the MD simulation [27] are used as observation data in the EnKF. The essential aspects of the MD simulation are briefly described below.

The interatomic interaction between Fe atoms was represented using the FS potential [42]. The pure Fe melt was obtained by heating a bcc crystal consisting of 1 037 880 Fe atoms with a size of $53.4 \times 53.4 \times 4.3\,\mathrm{nm}^3$ ($186 \times 186 \times 15$ unit cells) up to 3500 K under a constant *NVT* condition. The solid particle of the bcc crystal was then inserted into the melt. This system was annealed under zero pressure and a constant *NPT* condition at various degrees of undercooling ΔT.

Figures 1(a) and 2(a) shows snapshots of the MD simulation for $\Delta T = 200$ and 300 K, respectively. The solid (blue) and liquid (gray) atoms are distinguished on the basis of common neighbor analysis [29]. The vertical and horizontal axes correspond to $\langle 100\rangle$ of the bcc crystal located in the center part of the system. In both cases, preferential growth of the solid takes place slightly in the $\langle 100\rangle$ direction, resulting in a slight deviation from the circle shape expected in the case of isotropic interfacial properties. It is important to note that the interface shape largely fluctuates during the growth processes.

All the interfacial parameters in Eq. (2) should be evaluated by analyzing the growth processes shown in Figs. 1(a) and 2(a). For instance, time changes of the local velocity and interface curvature are measured in different crystallographic orientations. Then the four parameters in Eq. (2) can be evaluated on the basis of the relationship between the local velocity and the curvature by minimizing a cost function, e.g., the mean square error. However, such simple parameter fitting procedures are ineffective and inaccurate in the present case, because very strong fluctuation of the interface shape occurs at the atomistic level; accordingly, the local velocity and curvature fluctuate strongly, which causes extremely high uncertainty in the parameter fitting based on minimization of the cost function. In other words, the effect of the noise term ζ in Eq. (2) is extremely high at this scale, which hampers accurate determination of the interface dynamics. How to treat fluctuation at the atomistic scale within the continuum description is an essential problem in multiscale analysis. To solve this problem, this study treats the data of MD simulation as stochastic variables and the interfacial properties are probabilistically estimated on the basis of a Bayesian filtering method, i.e., the EnKF, which will be explained in Sec. V. More specifically, the results of MD simulation are assimilated into the phase-field simulation described in Sec. III to estimate the interfacial parameters. To this end, we convert the MD data into the diffuse-interface description, as explained below.

The output data of the MD simulation are the velocity and spatial coordinates of the atoms. Such data are not suitable for data assimilation with the phase-field model. In

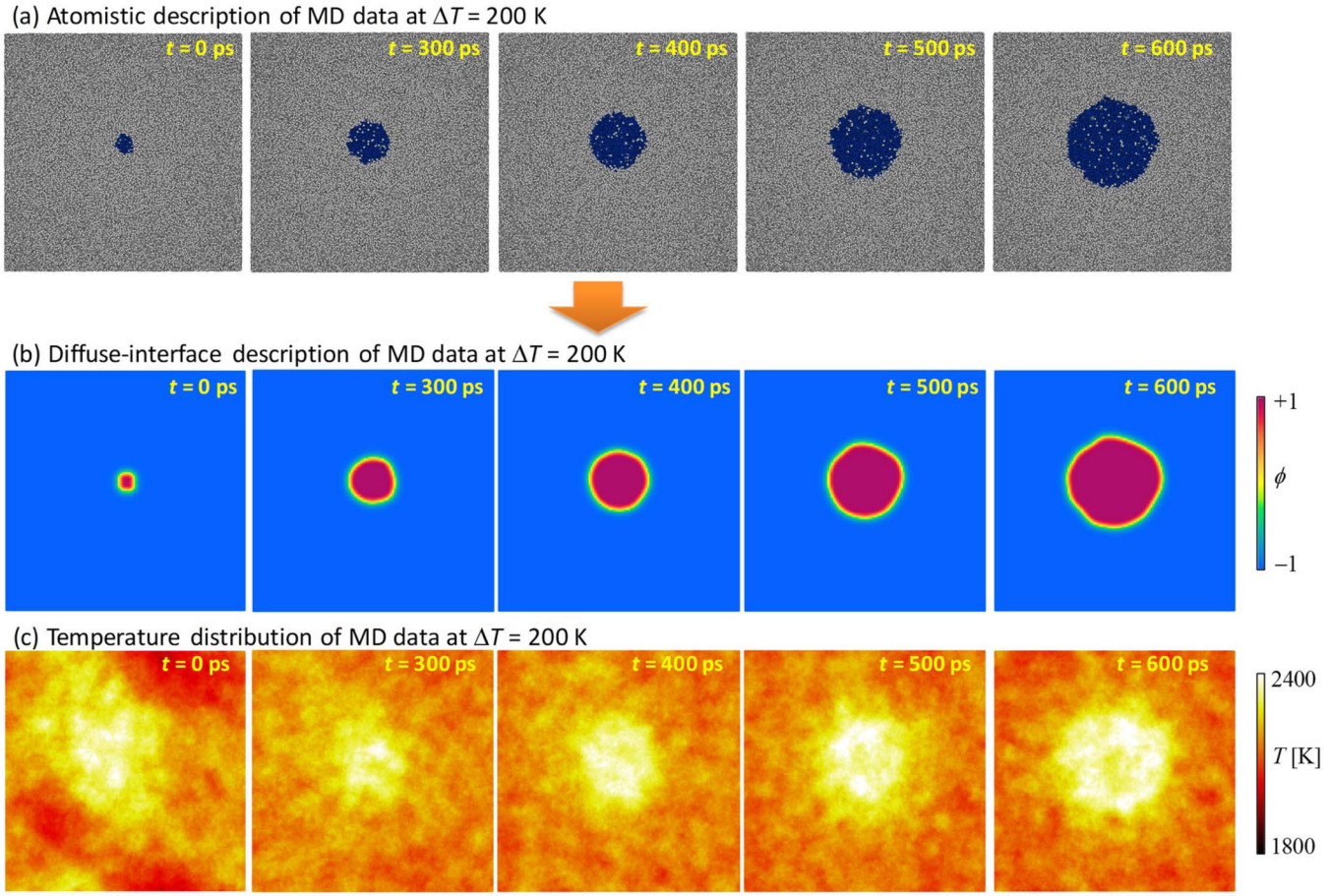

FIG. 1. Result of MD simulation for growth of a single solid in an undercooled melt of pure Fe at $\Delta T = 200$ K [27]. (a) Atomistic description of data where the solid and liquid atoms are shown in blue and gray, respectively. The vertical and horizontal axes correspond to ⟨100⟩ of the crystal. (b) Diffuse-interface description (phase-field profile) converted from the MD data in (a) in a domain consisting of 128 × 128 grid points. (c) Temperature distribution calculated from the local velocity of atoms in the MD simulation.

this study, the MD data were converted into the phase-field profile on the basis of a method developed previously [43] to assimilate the MD data into the phase-field simulation. Atoms in a bcc configuration were first identified by the common neighbor analysis. A cross section ($53.4 \times 53.4\,\mathrm{nm}^2$) of the MD computational system was divided into 2D square grid points. Then the phase-field variable ϕ was set to -1 for a liquid and $+1$ for a solid. The sharp-interface profile thus obtained was relaxed to get the diffuse interface by solving the phase-field equation without the curvature effect and driving force. This data conversion was carried out for the time series of the MD data. The results of the converted MD data for $\Delta T = 200$ and 300 K are shown in Figs. 1(b) and 2(b), respectively. The size and shape of the growing solid are reproduced well in the diffuse-interface description for both cases. These data of ϕ are used in the EnKF.

Note that only the temperature spatially averaged over the entire system was controlled to be constant with the *NPT* ensemble in the previous MD simulation [27]. This does not guarantee that the temperature is completely uniform during solidification because of the release of latent heat. The temperature distributions calculated from the velocity distributions of the atoms at $\Delta T = 200$ and 300 K are shown in Figs. 1(c) and 2(c), respectively. The temperature is not completely uniform in both cases and it is high in the solid because of the release of latent heat. In particular, in the late stage at $\Delta T = 300$ K, the difference between the temperatures in the solid and liquid regions becomes remarkable. Hence, the heat diffusion equation must be coupled with Eq. (3) in the parameter estimation. However, the time changes of temperature shown in Figs. 1(c) and 2(c) cannot simply be described by the heat diffusion equation with the usual boundary conditions, because only the spatially averaged temperature was controlled to be constant using the thermostat in the MD simulation [27]. Furthermore, another problem arises even if one can accurately describe the time change of temperature. As the interfacial parameters depend on the temperature, their spatial and temporal variations occur inside the interface according to the temperature distribution and such changes must be handled by introducing new coupling terms between ϕ and T in Eq. (3). Hence, the parameter estimation becomes extremely complicated. These problems are readily resolved when one employs MD data for completely isothermal solidification. In this attempt to develop an approach for computing the interfacial parameters on the basis of the EnKF, we introduce a simplification of u_{int} as described below.

Figures 3(a) and 3(b) show the time changes of u_{int} averaged over the interface region ($-0.999 < \phi < 0.999$)

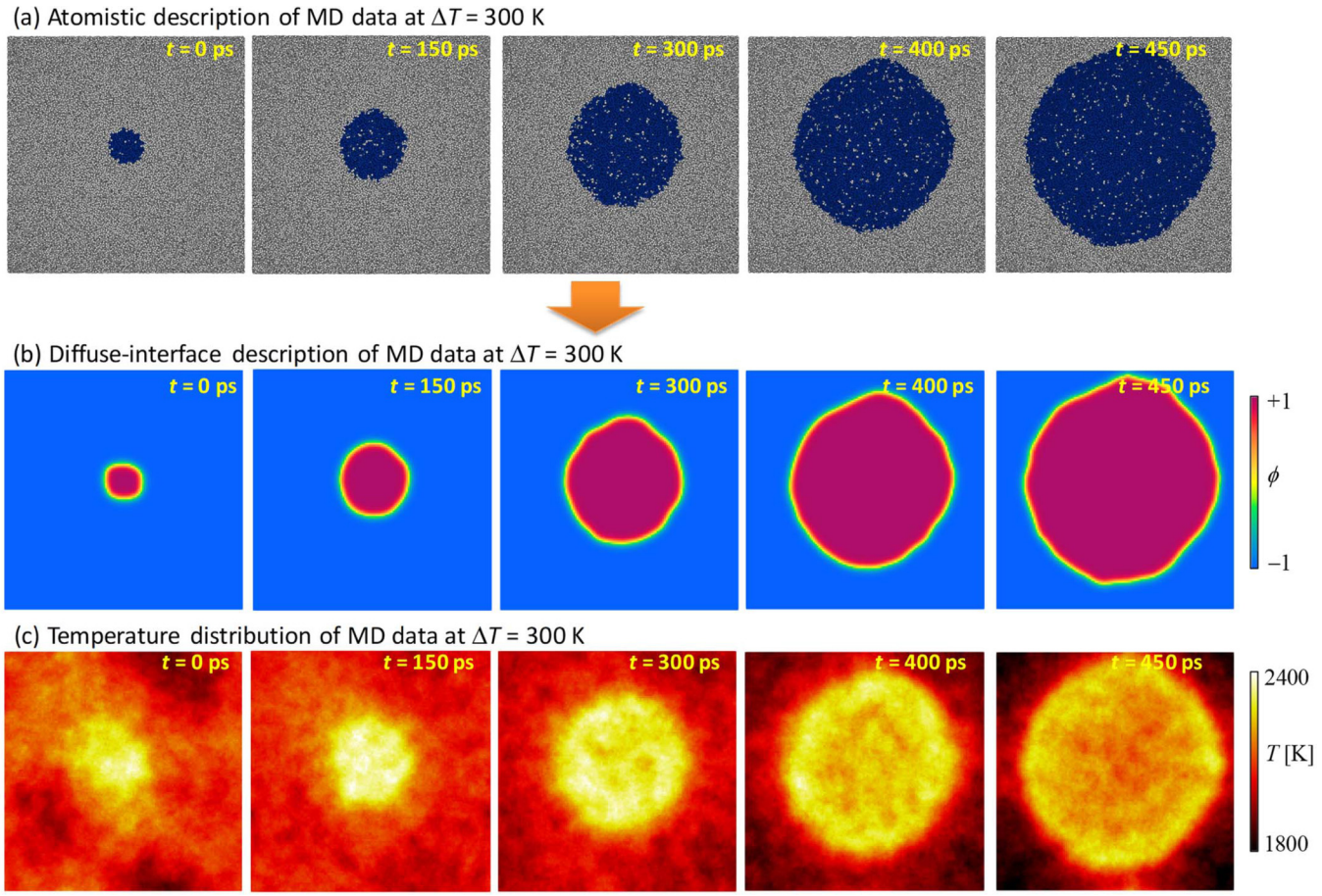

FIG. 2. Result of MD simulation for growth of a single solid in an undercooled melt of pure Fe at $\Delta T = 300\,\mathrm{K}$ [27]: (a) atomistic description, (b) diffuse-interface description (phase-field profile), and (c) temperature distribution.

obtained from the MD simulation for $\Delta T = 200$ and 300 K, respectively. Furthermore, the radius of the circle that has an area equivalent to that of the solid r_{ec} is shown in each figure. In the case of $\Delta T = 200$ K, u_{int} takes a nearly constant value during the solidification and stable growth of the solid occurs after around $t = 150$ ps. Therefore, we have decided to employ the MD data from 200 to 500 ps as the observation data in the parameter estimation for $\Delta T = 200$ K. The time-averaged value of u_{int} is calculated as $u_{\mathrm{int}} = -0.15$ and it is used in the phase-field simulation in the EnKF for simplicity. In the case of $\Delta T = 300\,\mathrm{K}$, the growth takes place from the beginning and u_{int} takes a nearly constant value until $t = 300$ ps. Hence, the MD data from 0 to 300 ps are used as the observation data in the case of $\Delta T = 300\,\mathrm{K}$. The value of u_{int} averaged over this time period is calculated as -0.23 and it is used in the phase-field simulation. Such simplification of u_{int} is introduced in this study to avoid the cumbersome problems associated with the time change of temperature distribution. Note that truly isothermal processes over the entire system must be realized by controlling the local velocities of the atoms, i.e., using a local thermostat in the MD simulation. In such cases, the degree of undercooling set as a computational condition can be directly employed in the phase-field simulation without analysis of the temperature distribution.

V. ENSEMBLE KALMAN FILTER

Data assimilation provides a methodology for integrating observation data and the simulation model to estimate the state of the system and/or the parameters governing the dynamics of interest. Because it achieves a reasonable trade-off between accuracy and computational cost, the EnKF has been used in various fields, such as oceanography and meteorology [32–34]. Our objective is to estimate σ_0, ε_c, β_0, and ε_k in Eq. (3) using the data of MD simulation (Figs. 1 and 2) as the observation data.

The EnKF is a method based on the Monte Carlo approximation of the Kalman filter. It is an ensemble-based method in which a number of simulations are conducted for different parameters and/or different initial states and these simulations correspond to ensemble members for approximating the probability distribution function of the state. In the EnKF, the state variable, model parameters of interest, and observation data are treated as stochastic variables and the estimation is conducted in a probabilistic manner. The EnKF consists of cycles of a forecast stage and an analysis stage (see Fig. 4). The simulations are independently and simultaneously carried out in the forecast stage, while the simulations are correlated with each other in the analysis stage. In the analysis stage, the parameters and state variables in the simulations are updated by the filtering procedure on the basis of the observation data.

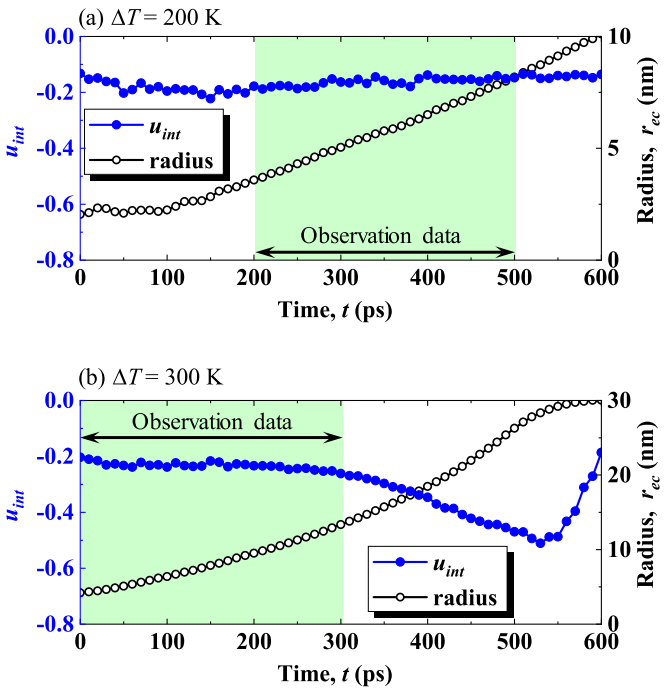

FIG. 3. Time changes of the dimensionless undercooling at the interface $u_{\rm int}$ and the equivalent-circle radius of the solid $r_{\rm ec}$ obtained from the MD simulation for (a) $\Delta T = 200\,\mathrm{K}$ and (b) $\Delta T = 300\,\mathrm{K}$. The arrows indicate the ranges of the data employed in the data assimilation.

Repeating this cycle gradually minimizes the expectation values of the variance-covariance matrix composed of the differences between the observation data and the simulation results.

In the forecast stage, the time evolution of the states is calculated as [34]

$$\mathbf{x}_i^f(t_n) = F\left(\mathbf{x}_i^a(t_{n-1})\right) + \boldsymbol{v}_i(t_n) \quad \text{for } i = 1, 2, \ldots, M, \tag{10}$$

where t_n represents a discrete time where the observation data are available and $\mathbf{x}_i^a(t_n)$ is the state vector (column vector) of the ensemble member i at time t_n, containing all the state variables at t_n. In the present case, $\mathbf{x}_i^a(t_n)$ is composed of the phase-field variables ϕ at all the discrete spatial points at t_n in the phase-field simulation specified by i, M is the total number of ensemble members, and F is a nonlinear operator describing the time evolution of the states from time t_{n-1} to t_n. Hence, F is given by the time evolution equation of ϕ [Eq. (3)] in the present case. Note that the superscripts a and f in the state vector [$\mathbf{x}_i^a(t_n)$ and $\mathbf{x}_i^f(t_n)$] indicate the analysis and forecast values, respectively. Further, $\boldsymbol{v}_i(t_n)$ is the system noise that accounts for the uncertainty of the model, i.e., the uncertainty of the dynamics originating from physics and/or factors that are not explicitly described in the operator F (the phase-field model). In addition, $\boldsymbol{v}_i(t_n)$ is given as Gaussian noise with zero mean and a covariant matrix $\boldsymbol{Q}_v$ and it is expressed as $\boldsymbol{v}_i(t) \sim N(0, \boldsymbol{Q}_v)$. Note that the parameters to be estimated are included in the state vectors $\mathbf{x}_i^a$ and $\mathbf{x}_i^f$. In other words, the state vector contains σ_0, ε_c, β_0, and ε_k as well as ϕ. The operator F for the interfacial parameters is the identity operator.

The forecast stage is followed by the filtering operation in the analysis stage. In the filtering, $\mathbf{x}_i^f(t_n)$ is updated as [32–34]

$$\mathbf{x}_i^a(t_n) = \mathbf{x}_i^f(t_n) + \mathbf{K}(t_n)\left[\mathbf{y}_{\rm obs}(t_n) + \delta\boldsymbol{\omega}_i(t_n) - \mathbf{H}\mathbf{x}_i^f(t_n)\right] \quad \text{for } i = 1, 2, \ldots, M, \tag{11}$$

where $\boldsymbol{y}_{\rm obs}(t_n)$ represents the observation data corresponding to the values of ϕ at different positions obtained from the MD simulation [Figs. 1(b) and 2(b)], $\mathbf{H}$ is the observation matrix that yields the values corresponding to the observation data for $\mathbf{x}_i^f(t_n)$, and $\mathbf{K}(t_n)$ is the Kalman gain given by

$$\mathbf{K}(t_n) = \mathbf{V}(t_n)\mathbf{H}^T\left[\mathbf{H}\mathbf{V}(t_n)\mathbf{H}^T + \mathbf{R}(t_n)\right]^{-1}, \tag{12}$$

where the superscript T indicates the transpose of the matrix (or vector) and $\mathbf{V}(t_n)$ is the sample covariance matrix given by

$$\mathbf{V}(t_n) = \frac{1}{M-1}\sum_i^M \delta\mathbf{x}_i^f(t_n)\left[\delta\mathbf{x}_i^f(t_n)\right]^T, \tag{13}$$

with $\delta\mathbf{x}_i^f(t_n) = \mathbf{x}_i^f(t_n) - \langle\mathbf{x}_i^f(t_n)\rangle$, where angular brackets represent the ensemble average. In addition, $\mathbf{R}(t_n)$ in Eq. (12) is the observation error covariance matrix given by

$$\mathbf{R}(t_n) = \frac{1}{M-1}\sum_{i=1}^M \delta\boldsymbol{\omega}_i(t_n)[\delta\boldsymbol{\omega}_i(t_n)]^T, \tag{14}$$

TABLE I. Values of hyperparameters tested in this study.

Hyperparameters	Values
number of ensemble members M	128, 256, 512, 1024, 2048
time interval of filtering $\Delta t_{\rm obs}$ (ps)	1–300
variance of observation noise Q_R	1–40
parameter proportional to variance of noise for ϕ, a_R	0–40
variance of noise for σ_0	$0-1\times10^{-3}$
variance of noise for ε_c	$0-1\times10^{-6}$
variance of noise for β_0	0–0.01
variance of noise for ε_k	$0-1\times10^{-6}$
maximum of initial values of σ_0 and $\sigma_{0,\max}$ (J/m^2)	0.1–0.8
maximum of initial values of ε_c and $\varepsilon_{c,\max}$	0.01–0.04
maximum of initial values of β_0 and $\beta_{0,\max}$ (s/m)	0.01–0.1
maximum of initial values of ε_k and $\varepsilon_{k,\max}$	0.01–0.4

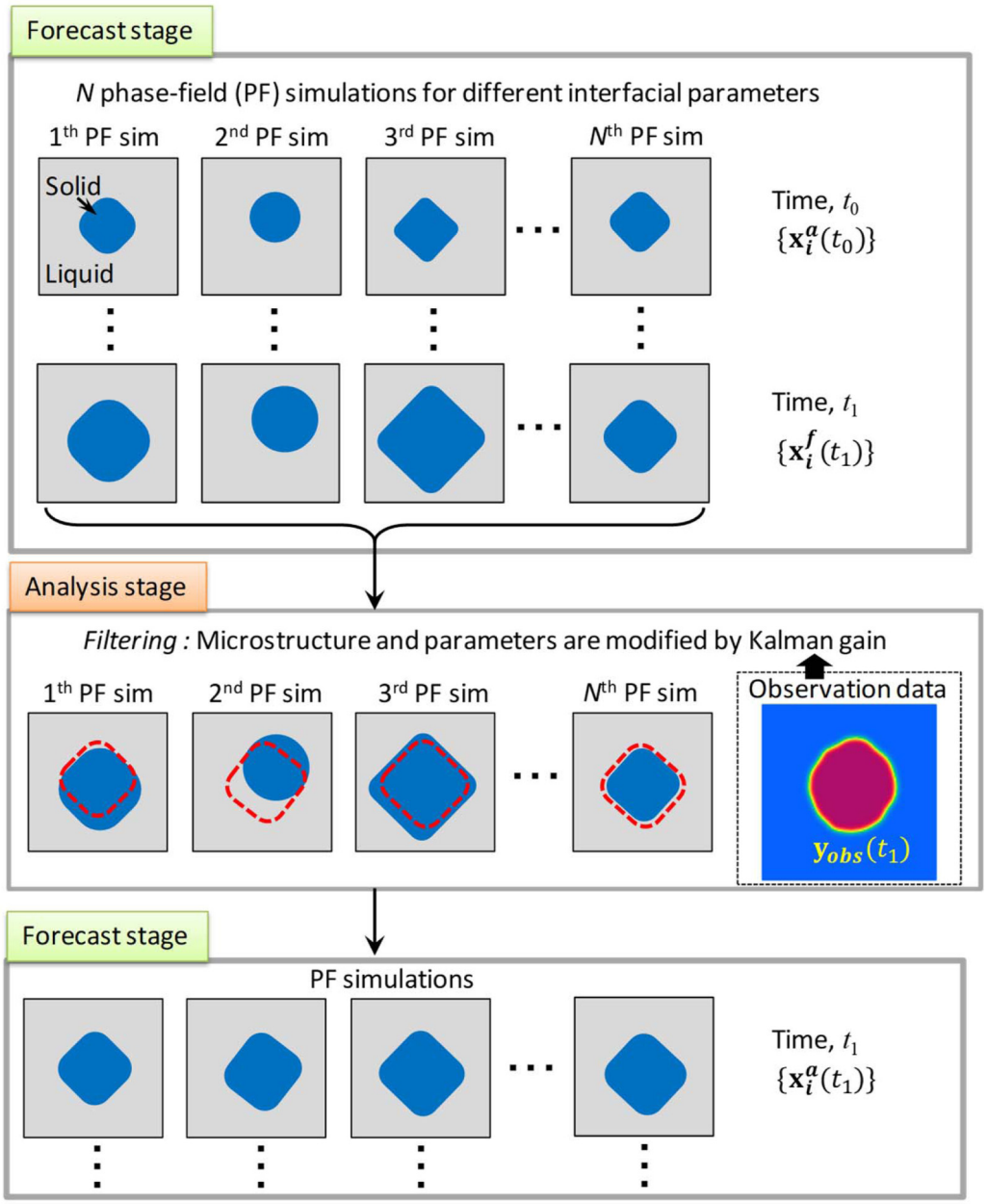

FIG. 4. Schematic illustration of forecast and analysis stages in the EnKF.

where $\delta\boldsymbol{\omega}_i(t_n) = \boldsymbol{\omega}_i(t_n) - \langle\boldsymbol{\omega}_i(t_n)\rangle$ and $\boldsymbol{\omega}_i(t_n)$ is the observation noise, i.e., the error included in the observation data, given by $\boldsymbol{\omega}_i(t_n) \sim N(0, \mathbf{R}(t_n))$. In this ensemble approximation, the probability distribution function for state $\mathbf{x}(t_n)$, $\rho(\mathbf{x}(t_n))$, can be approximated as

$$\rho(\mathbf{x}(t_n)) = \frac{1}{M}\sum_{i=1}^{M}\delta\big(\mathbf{x}(t_n) - \mathbf{x}_i^a(t_n)\big). \tag{15}$$

By repeating the forecast and analysis stages, the parameters and state variables approach the true values (the most probable values). The expectation values of the parameters are obtained from the ensemble average of the parameters at each filtering step. The estimated value of each parameter can be obtained by time-averaging the expectation value in the late time period.

Many variants on the EnKF algorithm have been developed to achieve higher efficiency and accuracy of the EnKF. By carrying out the twin experiments, in this study, we determined the suitable algorithm and optimal conditions of the EnKF as explained below. First, diagonalization of the matrix $\mathbf{R}(t_n)$ given by Eq. (14) is generally a good approximation [44]; hence, we treated it as a diagonal matrix, which accelerates the computation of the inverse matrix in Eq. (12). Then $\mathbf{R}$ is represented as $\mathbf{R} = Q_R\mathbf{I}$ with the identity matrix $\mathbf{I}$ and variance Q_R. We investigate the effect of Q_R on the estimation accuracy. In addition, the noise term for ϕ in Eq. (3) was regarded as the system noise in Eq. (10) and the effect of a_R on the estimation accuracy is investigated. Similarly, small Gaussian noise was added to the interfacial parameters during the time evolution of the system, which was regarded as the system noise. Its variance is denoted by Q_σ for σ_0,

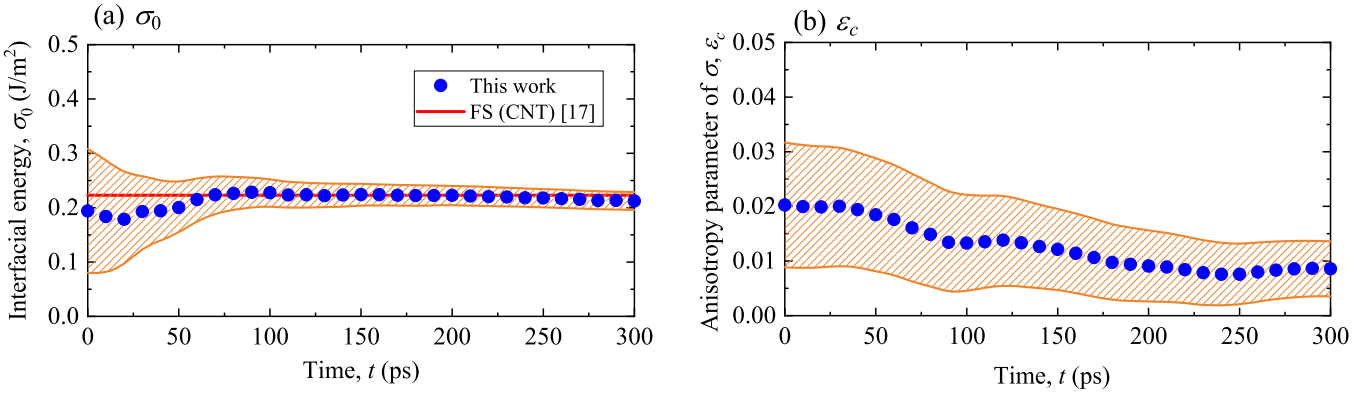

FIG. 5. Example of estimated result of two parameters (a) σ_0 and (b) ε_c on the basis of the EnKF with MD data at $\Delta T = 200$ K ($u_{\rm int} = -0.15$). Here β_0 and ε_k were set to 6.15×10^{-3} s/m and 0.085, respectively [17]. The estimation condition was given as $Q_R = 4$, $a_R = 10$, $Q_\sigma = 1.0 \times 10^{-4}$, $Q_c = 1.0 \times 10^{-6}$, $\sigma_{0,\max} = 0.4\,{\rm J/m^2}$, and $\varepsilon_{c,\max} = 0.04$.

Q_c for ε_c, Q_β for β_0, and Q_k for ε_k and its effects on the accuracy were examined. Furthermore, the initial values of the interfacial parameters are randomly set with the prescribed upper limits. The upper limits of the interfacial parameters in the initial random setting are denoted by $\sigma_{0,\max}$, $\varepsilon_{c,\max}$, $\beta_{0,\max}$, and $\varepsilon_{k,\max}$, and the effects of these upper limits on the estimation accuracy are investigated. The filtering time interval $\Delta t_{\rm obs}$ is also important for accurate estimation and its effect is investigated. Finally, the number of ensemble members M is varied to obtain the optimal condition on the basis of the trade-off between accuracy and computational cost. The ranges of the parameters investigated in this study are summarized in Table I, and these parameters are called hyperparameters.

In this study, estimation using MD data is referred to as actual estimation to distinguish it from the estimation in the twin experiments. All the computations of the twin experiments and the actual estimation are performed three times for each condition using different seeds for the noise terms. Furthermore, all the computations are accelerated using a GPU (Tesla P100).

VI. RESULTS AND DISCUSSION

A. Twin experiments and estimation accuracy

We carried out the twin experiments to clarify the optimal values of some hyperparameters for accurate estimation. First, the number of ensemble members M was changed from 128 to 2048 with several sets of hyperparameters. Although the estimation accuracy gradually increases with M, there is no significant difference when $M \geqslant 512$. Hence, M was set to 512 in the twin experiments. We tested the effects of the time interval of filtering $\Delta t_{\rm obs}$ on the estimation accuracy and found that the accuracy increases as $\Delta t_{\rm obs}$ decreases. However, when $\Delta t_{\rm obs}$ is extremely small, there is a slight change in the microstructure between the filtering steps, which results in low accuracy. Thus, $\Delta t_{\rm obs}$ was set to 10 ps in the twin experiments.

The optimal values of the other hyperparameters can be determined in the twin experiments. However, the optimal set of values was found to depend on the magnitude of the observation noise, i.e., Q_R. It is extremely difficult to determine the appropriate value of Q_R prior to the actual estimation. Hence, we carried out a number of actual estimations using different values of Q_R and different sets of the other hyperparameters. As the estimation result depends on the values of the hyperparameters, it is necessary to evaluate the accuracy of the result in the actual estimation. Therefore, we seek a quantity related to the accuracy of the result in the twin experiments. We found that the accuracy of the result monotonically increases with the likelihood Z defined as

$$Z = \left\langle \exp\left(-\frac{\Delta E}{Q_R}\right)\right\rangle, \tag{16}$$

where ΔE is given by $\Delta E = (\mathbf{y}_{\rm obs} - \mathbf{H}\mathbf{x}_i^a)^T(\mathbf{y}_{\rm obs} - \mathbf{H}\mathbf{x}_i^a)$. In this study, therefore, the accuracy of the result of the actual estimation is evaluated on the basis of Z according to Eq. (16).

B. Simultaneous estimation of all interfacial parameters from MD simulation

Before conducting simultaneous estimation of the four interfacial parameters, we tested the estimation of two parameters to investigate the feasibility of the present approach. It should be instructive to demonstrate the result of testing the estimation of two parameters, namely, σ_0 and ε_c. In a previous study, β_0 and ε_k of pure Fe were computed by analyzing the solid-liquid interfacial motion in an undercooled melt via MD simulation with the FS potential [17]. The computed values were $\beta_0 = 6.15 \times 10^{-3}$ s/m and $\varepsilon_k = 0.085$, which were obtained by taking the averages in a temperature range. We considered that these average values of β_0 and ε_k do not significantly differ from the true values below T_m. Therefore, to check the feasibility of the approach, we examined only σ_0 and ε_c with the MD data at $\Delta T = 200$ K ($u_{\rm int} = -0.15$) by assuming $\beta_0 = 6.15 \times 10^{-3}$ s/m and $\varepsilon_k = 0.085$. An example of the result is shown in Fig. 5. The estimation condition is given as $Q_R = 4$, $a_R = 10$, $Q_\sigma = 1.0 \times 10^{-4}$, $Q_c = 1.0 \times 10^{-6}$, $\sigma_{0,\max} = 0.5\,{\rm J/m^2}$, and $\varepsilon_{c,\max} = 0.04$. In each figure, the horizontal axis represents the time. Note that the observation data from $t = 200$ to 500 ps in Fig. 3 (a) are employed in the EnKF. Hence, the estimation starts from the microstructure at $t = 200$ ps; accordingly, $t = 0$ ps in Fig. 5 corresponds to $t = 200$ ps in Fig. 3(a). The circle represents the expectation

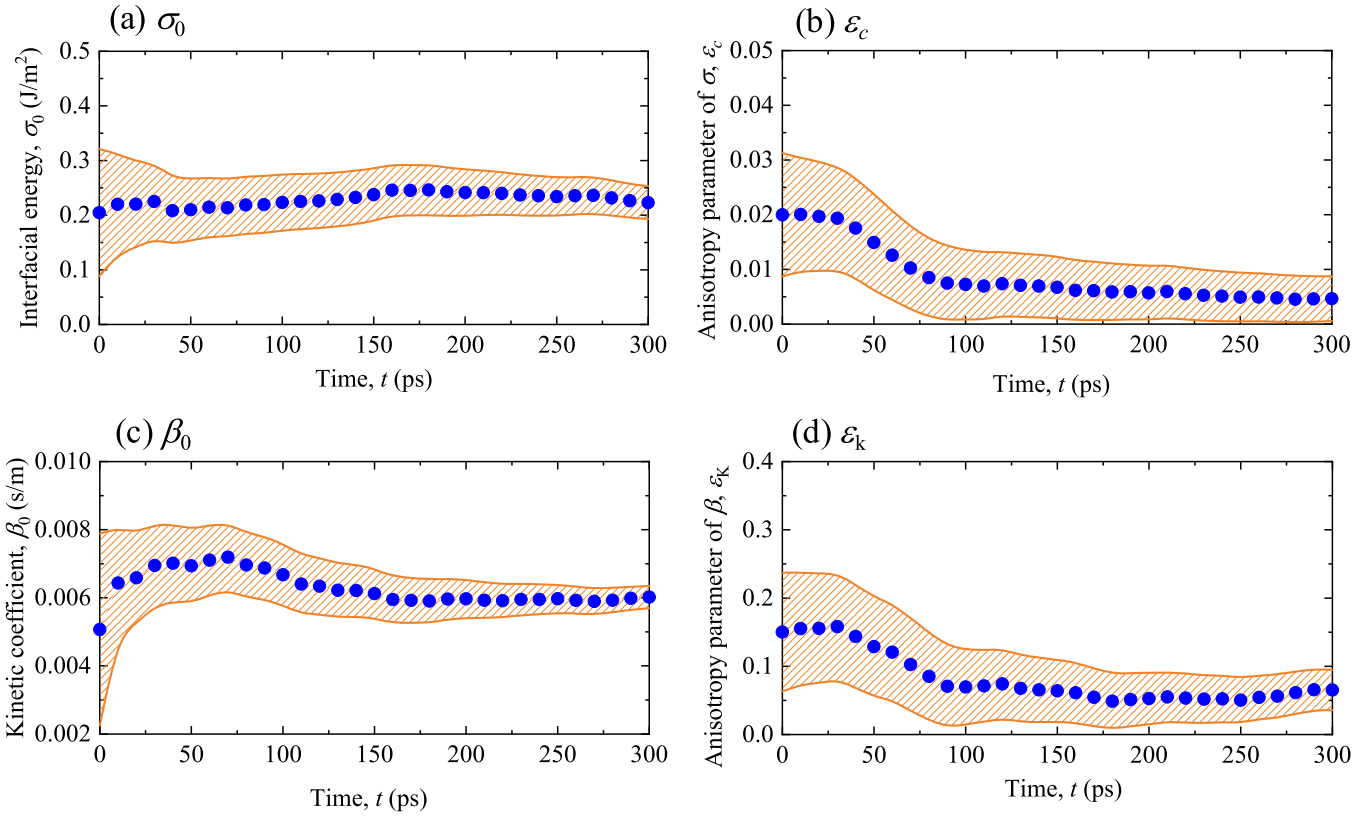

FIG. 6. Example of simultaneous estimation of the four interfacial parameters on the basis of the EnKF with MD data at $\Delta T = 200$ K ($u_{\rm int} = -0.15$): (a) σ_0, (b) ε_c, (c) β_0, and (d) ε_k. The estimation condition was given as $Q_R = 1$, $a_R = 5$, $Q_s = Q_c = Q_b = Q_k = 0$, $\sigma_{0,\max} = 0.4\,{\rm J/m^2}$, $\varepsilon_{c,\max} = 0.04$, $\beta_{0,\max} = 0.01$ s/m, and $\varepsilon_{k,\max} = 0.3$.

value at each filtering step and the hatched area indicates the range of standard deviation. In Fig. 5(a), the red horizontal line indicates the value of σ_0 obtained by MD simulation with the FS potential on the basis of the classical nucleation theory (CNT) [17] and it represents the average value in a temperature range. This value is slightly higher than the original value because the liquid density was recalculated for computing σ_0 in this study. The estimated value of σ_0 based on the present approach becomes nearly constant after 80 ps and its constant value is in good agreement with the data of the previous MD simulation [17]. Although σ_0, β_0, and ε_k reported in the previous study [17] are the average values in the temperature ranges and thereby this testing is not rigorous, the good agreement shown in Fig. 5(a) strongly indicates that the present approach is feasible and accurate. Actually, as shown later, σ_0, β_0, and ε_k estimated at this undercooling temperature on the basis of the present approach are comparable to these literature data [17]. In Fig. 5(b), the estimated value of ε_c gradually decreases with time and it exhibits no significant change in the late time period, approaching $\varepsilon_c \approx 8.6 \times 10^{-3}$. It is found that this value of ε_c does not depend significantly on the values of the hyperparameters that we tested; hence, it can be regarded as the estimated value. This result implies that the anisotropy of the interfacial energy can be estimated in the present approach, even though only a slight anisotropy in the shape of a solid appears in the MD simulation adopted in this study [Fig. 1(b)]. Furthermore, if one takes a different view of Fig. 5, it demonstrates that the result of MD simulation for the growth of a single solid [27] can be explained by the Gibbs-Thomson relation described by Eq. (2) or (3) with the interfacial parameters independently obtained from different MD simulations, i.e., σ_0 based on CNT analysis [17], β_0 and ε_k based on analysis of the moving interface [17], and $\varepsilon_c \approx 8.6 \times 10^{-3}$ based on the EnKF.

Let us focus on the results of the simultaneous estimation of all the interfacial parameters. Figures 6 and 7 show examples of actual estimations of the four parameters with MD data at $\Delta T = 200$ K ($u_{\rm int} = -0.15$) and $\Delta T = 300$ K ($u_{\rm int} = -0.23$), respectively. The estimation conditions are given as $Q_R = 1$, $a_R = 5$, $Q_s = Q_c = Q_b = Q_k = 0$, $\sigma_{0,\max} = 0.4\,{\rm J/m^2}$, $\varepsilon_{c,\max} = 0.04$, $\beta_{0,\max} = 0.01$ s/m, and $\varepsilon_{k,\max} = 0.3$ in the former case and $Q_R = 10$, $a_R = 10$, $Q_\sigma = 1 \times 10^{-4}$, $Q_c = 1 \times 10^{-6}$, $Q_\beta = 1 \times 10^{-5}$, $Q_k = 1 \times 10^{-7}$, $\sigma_{0,\max} = 0.6\,{\rm J/m^2}$, $\varepsilon_{c,\max} = 0.04$, $\beta_{0,\max} = 0.01$ s/m, and $\varepsilon_{k,\max} = 0.1$ in the latter case. The horizontal axis represents the time. The circle represents the expectation value at each filtering step and the hatched area indicates the range of standard deviation. Note that all the parameters take nearly constant values in the late stage ($t >\sim 200$ ps) in both cases. Hence, the estimated values of the parameters are determined by averaging the expectation values after 200 ps. The results shown in Figs. 6 and 7 demonstrate that all the interfacial parameters at a given undercooling temperature can be simultaneously estimated from a single MD simulation. We emphasize that these values are not equilibrium values at T_m but the values at $u_{\rm int} = -0.15$ (Fig. 6) and $u_{\rm int} = -0.23$ (Fig. 7). Therefore, these values are

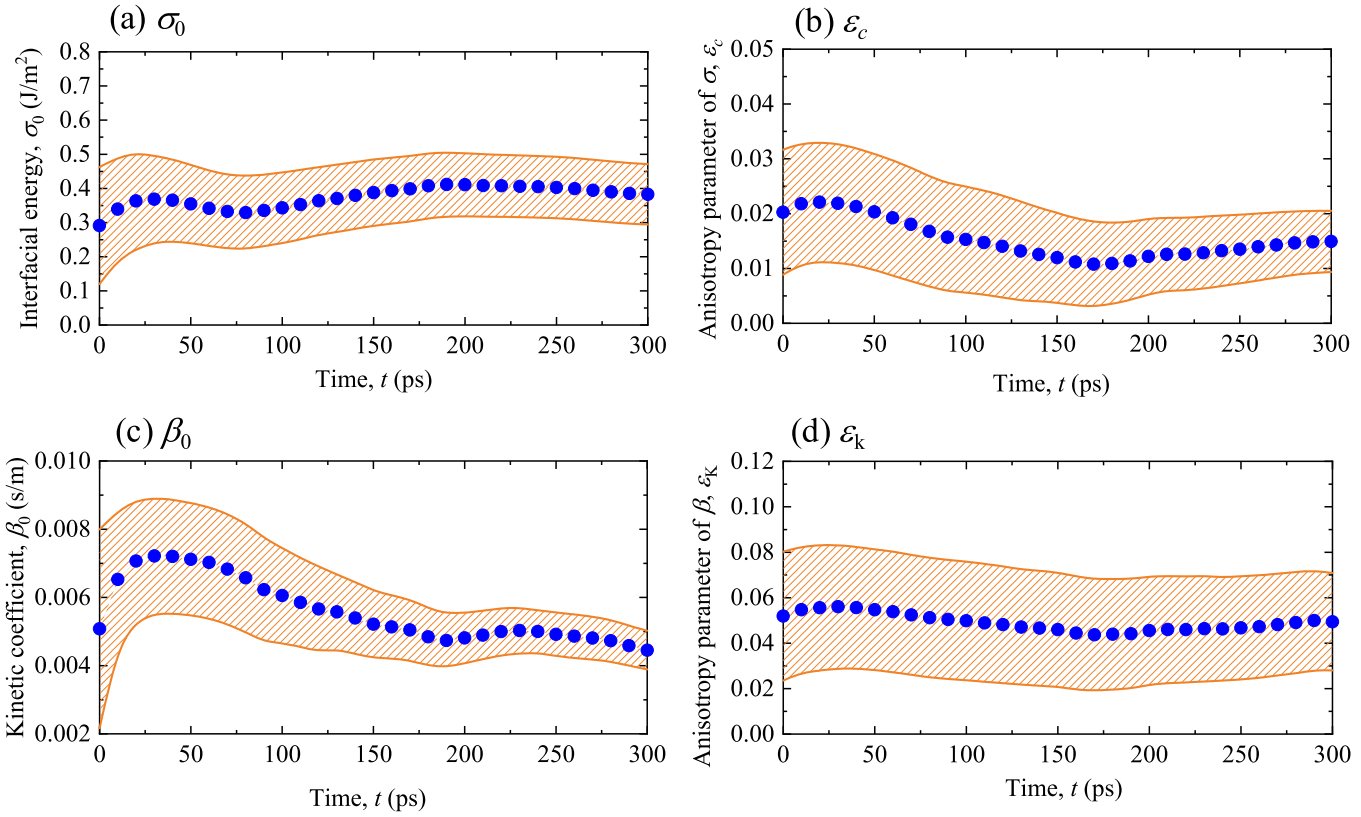

FIG. 7. Example of simultaneous estimation of the four interfacial parameters on the basis of the EnKF with MD data at $\Delta T = 300\,\mathrm{K}$ ($u_{\mathrm{int}} = -0.23$): (a) σ_0, (b) ε_c, (c) β_0, and (d) ε_k. The estimation condition was given as $Q_R = 10$, $a_R = 10$, $Q_\sigma = 1 \times 10^{-4}$, $Q_c = 1 \times 10^{-6}$, $Q_b = 1 \times 10^{-5}$, $Q_k = 1 \times 10^{-7}$, $\sigma_{0,\max} = 0.6\,\mathrm{J/m^2}$, $\varepsilon_{c,\max} = 0.04$, $\beta_{0,\max} = 0.01\,\mathrm{s/m}$, and $\varepsilon_{k,\max} = 0.1$.

employed for the simulation of solidification microstructures at these undercooling temperatures.

The estimation was carried out three times for each condition using different seeds of the noise terms. As described in the preceding section, the accuracy of the results is evaluated on the basis of Z given by Eq. (16). The actual estimation was carried out for three values of Q_R, i.e., $Q_R = 1$, 4, and 10; then the five most accurate results for each value of Q_R were selected from the results obtained for more than 100 different conditions. As the actual estimation was conducted three times for each condition, a total of 45 estimated data were averaged to obtain the final estimated value for each value of u_{int}.

C. Temperature dependence of interfacial parameters

Figure 8(a) shows the temperature dependence of σ_0 estimated by the EnKF. The two blue symbols represent the results of the present study. The green open rhombus represents the experimental value of pure Fe [3]. The other green symbols represent the literature data obtained from MD simulations with different potentials for Fe on the basis of the CFM, CT, or CNT [45,46]. These are plotted at T_m ($u_{\mathrm{int}} = 0$) because the simulations are carried out at T_m or near T_m. The dashed red line represents the result of MD simulation with the FS potential on the basis of the CNT [17]. In the

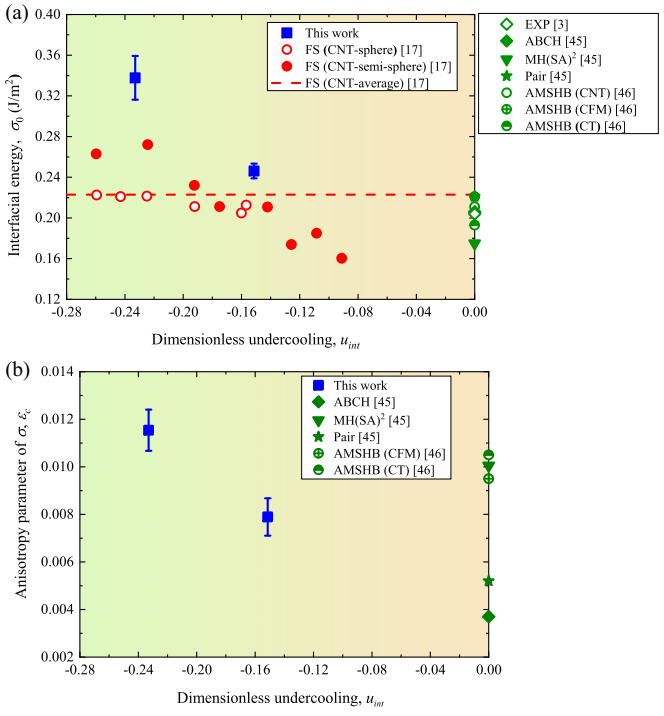

FIG. 8. Temperature dependences of (a) the interfacial energy σ_0 and (b) its anisotropy parameter ε_c.

previous study [17], the critical radius was computed for both a freestanding spherical crystal and a semispherical crystal on a substrate in the undercooled melt. In this study, these data are employed one by one to plot σ_0 at different temperatures. The open and closed red circles represent the values calculated at each temperature for the former and latter cases, respectively.

First, it is important to note that our result clearly shows that σ_0 decreases as the temperature increases, although there are only two data points. The negative temperature dependence can also be indicated by the closed red circles. Our result at $u_{\rm int} = -0.15$ is fairly close to the values recalculated from the literature data [17], while the value at $u_{\rm int} = -0.23$ is higher than the literature data [17]. The reason for this difference is not clear. In this study, we have simplified the value of $u_{\rm int}$ as described in Sec. IV, which may reduce the estimation accuracy. On the other hand, a large fluctuation at the atomistic scale generally makes it difficult to precisely measure the critical size of a solid in an undercooled melt in MD simulation, which may cause some uncertainty in the literature data [17].

As described in the Introduction, the temperature dependence of σ_0 has been explicitly or implicitly investigated in theoretical and numerical works [6–9,14,18–21,47]. It was found in all these works that σ_0 increases as the temperature increases in a relatively-low-temperature region. However, there is a difference in the behavior near T_m. Some works demonstrated the negative temperature dependence of σ_0 near T_m [20,21], while the other works showed the positive temperature dependence even near T_m [6–9,14,18,19,47]. It is not straightforward to clarify which dependence is correct by examining the validity of assumptions and/or simplifications made in the theoretical and numerical works one by one. Experimental determination of σ_0 has been conducted by means of several techniques such as the maximum nucleation undercooling (MU) technique [3], the dihedral angle, the contact angle, and the grain boundary groove techniques [4,48,49]. Although these techniques, except for the MU technique, were employed to determine σ_0 at T_m, the value of σ_0 derived from the MU technique represents the one at the nucleation temperature that is far below T_m. The values of the MU technique tend to be lower than the other experimental data measured at T_m [14]. This trend is indicative of the positive temperature dependence of σ_0. However, it is not clear whether this trend found at temperatures far below T_m can be applied to the temperature range near T_m. In addition, the effect of interface curvature on σ_0 [50] and the possibility of the appearance of the metastable phase(s) before crystallization of the primary phase may cause uncertainty in σ_0 derived from the nucleation undercooling experiment. The same uncertainty may be considered in numerical works based on the CNT [19]. In this respect, the recent approach based on metadynamics MD simulation [26] is expected to provide the reliable result for the temperature dependence of σ_0 because it enables the computation of σ for the planar solid-liquid interface at $T \neq T_m$ without relying on the CNT and the phenomenological assumptions. The metadynamics MD work for the Lennard-Jones system showed that the behavior of σ with T depends on the choice of reference state for computing the solid-liquid interface. Importantly, regardless of the reference states tested in the work, the negative temperature dependence of σ was computed for the (111) plane [26]. This result is consistent with our finding in this study. However, there are only two data points in the present results and, moreover, we have introduced the simplification of $u_{\rm int}$, which may cause estimation error of σ_0 in the present work. In this regard, additional information is explained below.

In Fig. 3(b), $u_{\rm int}$ approximately takes a constant value from 0 to about 300 ps and then it gradually decreases until about 550 ps. The estimation was accordingly conducted using the data from 0 to 300 ps because our focus is on the steady-state growth. In the preliminary investigation, on the other hand, we tested the data assimilation using the data from 0 to 550 ps. In such cases, the estimated value of σ_0 gradually increases as the time increases (i.e., as $u_{\rm int}$ decreases) in the late stage of the estimation. This behavior seems to be consistent with the negative temperature dependence shown in Fig. 8(a). Furthermore, although the MD data only at $\Delta T = 200$ and 300 K have been employed in the actual estimation in this study, the MD simulation was actually carried out at $\Delta T = 500\,{\rm K}$ in Ref. [27]. The data at $\Delta T = 500\,{\rm K}$ are not utilized in this study because $u_{\rm int}$ continuously decreases with time and hence the steady-state value of $u_{\rm int}$ cannot be obtained. In the preliminary investigation, however, the estimation was performed using the data at $\Delta T = 500\,{\rm K}$. In many cases for different estimation conditions, σ_0 gradually increases with the increase in time (thus with the decrease in $u_{\rm int}$). Although the results in the preliminary investigation are not the steady-state value and more careful analysis is necessary, these results support our finding. More detailed investigations are necessary to obtain conclusive evidence about the temperature dependence of σ_0, which is left for future work. The estimation accuracy in the present approach should be improved when the MD simulation data best suited for the present purpose are used as the observation data. For instance, one may expect more accurate results when using MD simulation data for a growth process in a larger system under completely isothermal conditions; this is a topic for future work. Although there is room for further investigation regarding the quantitative aspect, it is important to note that both our results and the literature data [17] demonstrate that $d\sigma_0/dT < 0$, which is consistent with previous theoretical studies [20,21] and numerical work [26].

Figure 8(b) shows the temperature dependence of ε_c. Our results are represented by the two blue symbols, while the literature data are represented by the green symbols. It is shown that ε_c obviously depends on the temperature. More specifically it decreases as the temperature increases. This negative temperature dependence of ε_c is comparable to the result of the phase-field crystal theory for a model alloy [12], although the literature data are not free from the effects of solute concentration.

The temperature dependences of β_0 and ε_k are shown in Figs. 9(a) and 9(b), respectively. In each figure, the blue symbols represent the present results, while the green symbols represent the literature data with different potentials for Fe. The dashed red lines represent the results of MD with the FS

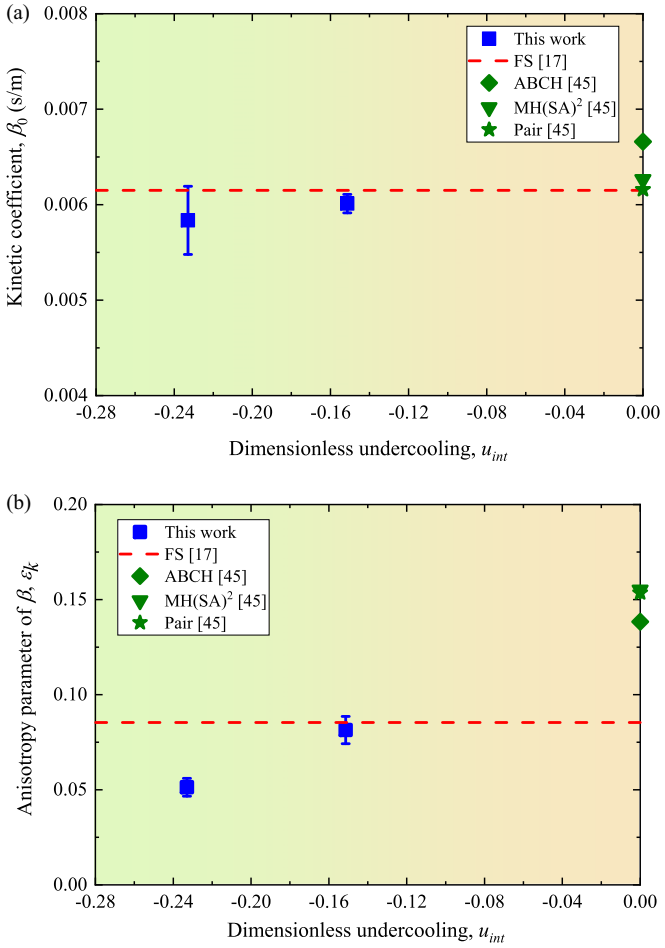

FIG. 9. Temperature dependences of (a) the kinetic coefficient β_0 and (b) its anisotropy parameter ε_k.

potential [17], which are averaged values over a wide temperature range. Our result shows that β_0 is nearly independent of the temperature in this temperature range. Importantly, the results are in good agreement with the data of Ref. [17], which strongly support the accuracy of the present estimation. In Fig. 9(b), ε_k increases with the temperature. The range of variation of ε_k estimated in this study is consistent with the result of the FS potential [17], which also supports the validity of the present data.

In summary, the present investigation demonstrated that $d\sigma_0/dT < 0$, $d\varepsilon_c/dT < 0$, $d\beta_0/dT \simeq 0$, and $d\varepsilon_k/dT > 0$ in the temperature range that we investigated. It is desirable to reveal the underlying mechanism of these behaviors in order to gain a deeper understanding of the interfacial properties. Also, understanding the mechanism may facilitate development of theoretical or numerical models for predicting the temperature dependences of these parameters. Such models can effectively be utilized for computing the interfacial parameters with high accuracy in combination with the present approach. Therefore, it is important to reveal the underlying mechanisms of the temperature dependences, even though it is beyond the scope of this study.

VII. CONCLUSION

Understanding and controlling evolution processes of solidification microstructures require the knowledge of solid-liquid interfacial properties out of equilibrium. Here we demonstrated an approach for computing the interfacial parameters out of equilibrium via MD simulation of microstructural processes. Since large fluctuations of the interface curvature and velocity appear at the atomistic scale, which causes high uncertainty in a simple parameter fitting, the results of MD simulations should be regarded as stochastic data at the microstructural level; thus, one needs a method for estimating the parameters on the basis of stochastic variables. In this study, we employed a data assimilation technique, namely, an ensemble Kalman filter, which allows simultaneous estimation of all the interfacial parameters in pure Fe at a given undercooling temperature from a single MD simulation. This is a multiscale approach that combines state-of-the-art techniques, data assimilation, large-scale MD, and phase-field simulations.

We investigated the temperature dependence of the interfacial parameters in pure Fe. Our analysis demonstrated that $d\sigma_0/dT < 0$, $d\varepsilon_c/dT < 0$, $d\beta_0/dT \simeq 0$, and $d\varepsilon_k/dT > 0$ in the temperature range that we investigated. Although the results of a previous MD simulation [27] were used as observation data in this study, it is important to find or develop MD simulation conditions best suited for the parameter estimation based on the EnKF to make the present approach more efficient and more accurate. This is an important topic for future work.

The rapid development of high-performance computing techniques has made it possible to scale up MD simulation to the level of small microstructures. Currently, the growth process of a single solid in an undercooled melt of pure material can readily be described by MD simulation at a reasonable computational cost. Also, it is easy to obtain the bulks' quantities by means of MD simulations with high accuracy. Once a set of hyperparameters is determined, the present approach enables simultaneous estimation of all interfacial parameters for a material of interest from such MD data in an automated manner. In particular, the single estimation of all parameters takes less than 30 min with a single GPU (Tesla P100) in the cases investigated in this study. Therefore, the present approach is considered very effective in terms of the computational cost as well as the applicability. We believe that the present approach will contribute to the advancement of our understanding of interfacial properties in a variety of materials.

ACKNOWLEDGMENTS

This research was partly supported by KAKENHI, Grants-in-Aid for Scientific Research (B) No. 19H02486 and (A) No. 17H01237. It was also supported in part by MEXT as a social and scientific priority issue (creation of new functional devices and high-performance materials to support next generation industries) to be tackled using the post-K computer.

[1] M. Asta, C. Beckermann, A. Karma, W. Kurz, R. Napolitano, M. Plapp, G. Purdy, M. Rappaz, and R. Trivedi, Acta Mater. **57**, 941 (2009).
[2] J. Zhang, S. O. Poulsen, J. W. Gibbs, P. W. Voorhees, and H. F. Poulsen, Acta Mater. **129**, 229 (2017).
[3] D. Turnbull, J. Appl. Phys. **21**, 1022 (1950).
[4] M. Gündüz and J. D. Hunt, Acta Mater. **33**, 1651 (1985).
[5] R. E. Napolitano and S. Liu, Phys. Rev. B **70**, 214103 (2004).
[6] R. H. Ewing, J. Cryst. Growth **11**, 221 (1971).
[7] F. Spaepen, Acta Metall. **23**, 729 (1975).
[8] L. Gránásy and M. Tegze, Mater. Sci. Eng. A **133**, 577 (1991).
[9] W. A. Curtin, Phys. Rev. Lett. **59**, 1228 (1987).
[10] S. R. Coriell and D. H. Turnbull, Acta Metall. **30**, 2135 (1982).
[11] L. V. Mikheev and A. A. Chernov, J. Cryst. Growth **112**, 591 (1991).
[12] B. A. Jugdutt, N. Ofori-Opoku, and N. Provatas, Phys. Rev. E **92**, 042405 (2015).
[13] A. Karma and D. Tourret, Curr. Opin. Solid State Mater. Sci. **20**, 25 (2016).
[14] J. J. Hoyt, M. Asta, and A. Karma, Mater. Sci. Eng. R **41**, 121 (2003).
[15] J.J. Hoyt, M. Asta, and A. Karma, Phys. Rev. Lett. **86**, 5530 (2001).
[16] R. L. Davidchack and B. B. Laird, Phys. Rev. Lett. **85**, 4751 (2000).
[17] Y. Watanabe, Y. Shibuta, and T. Suzuki, ISIJ Int. **50**, 1158 (2000).
[18] F. Spaepen, Mater. Sci. Eng. A **178**, 15 (1994).
[19] Z. Jian, N. Li, M. Zhu, J. Chen, F. Chang, and W. Jie, Acta Mater. **60**, 3590 (2012).
[20] R. Tognato, Phase Transit. **38**, 71 (1992).
[21] K. Mondal, A. Kumar, G. Gupta, and B. S. Murty, Acta Mater. **57**, 3422 (2009).
[22] F. Aqra and A. Ayyad, Appl. Surf. Sci. **257**, 6372 (2011).
[23] H. M. Lu and Q. Jiang, J. Phys. Chem. B **109**, 15463 (2005).
[24] A. Korner and G. Schoeck, Philos. Mag. A **61**, 909 (1990).
[25] R. Kikuchi and J. W. Cahn, J. Phys. Chem. Solids **23**, 137 (1962).
[26] B. Cheng, G. A. Tribello, and M. Ceriotti, Phys. Rev. B **92**, 180102(R) (2015).
[27] Y. Shibuta, K. Oguchi, and M. Ohno, Scr. Mater. **86**, 20 (2014).
[28] Y. Shibuta, S. Sakane, T. Takaki, and M. Ohno, Acta Mater. **105**, 328 (2016).
[29] Y. Shibuta, S. Sakane, E. Miyoshi, S. Okita, T. Takaki, and M. Ohno, Nat. Commun. **8**, 10 (2017).
[30] Y. Shibuta, M. Ohno, and T. Takaki, JOM **67**, 1793 (2015).
[31] Y. Shibuta, M. Ohno, and T. Takaki, Adv. Theory Simul. **1**, 1800065 (2018).
[32] G. Evensen, IEEE Control Syst. Mag. **29**, 83 (2009).
[33] P. J. Van Leeuwen, Mon. Weather Rev. **137**, 4089 (2009).
[34] P. L. Houtekamer and F. Zhang, Mon. Weath. Rev. **144**, 4489 (2016).
[35] K. Sasaki, A. Yamanaka, S. Ito, and H. Nagao, Comput. Mater. Sci. **141**, 141 (2018).
[36] A. Yamanaka, Y. Maeda, and K. Sasaki, Mater. Design **165**, 107577 (2019).
[37] R. Kobayashi, Exp. Math. **3**, 59 (1994).
[38] M. E. Glicksman, *Principles of Solidification* (Springer Science + Business Media, New York, 2011).
[39] J. Bragard, A. Karma, Y. H. Lee, and M. Plapp, Interface Sci. **10**, 121 (2002).
[40] A. Karma and W. J. Rappel, Phys. Rev. E **60**, 3614 (1999).
[41] B. Echebarria, A. Karma, and S. Gurevich, Phys. Rev. E **81**, 021608 (2010).
[42] M. W. Finnis and J. E. Sinclair, Philos. Mag. A **50**, 45 (1984).
[43] E. Miyoshi, T. Takaki, Y. Shibuta, and M. Ohno, Comput. Mater. Sci. **152**, 118 (2018).
[44] T. Miyoshi, TENKI **52**, 93 (2005).
[45] D. Y. Sun, M. Asta, and J. J. Hoyt, Phys. Rev. B **69**, 174103 (2004).
[46] J. Liu, R. L. Davidchack, and H. B. Dong, Comput. Mater. Sci. **74**, 92 (2013).
[47] Y. Sun, F. Zhang, H. Song, M. I. Mendelev, C. Z. Wang, and K.-M. Ho, J. Chem. Phys. **149**, 174501 (2018).
[48] M. E. Glicksman and C. L. Vold, Acta Metall. **17**, 1 (1969).
[49] V. Marasli and J. D. Hunt, Acta Mater. **44**, 1085 (1996).
[50] S. Prestipino, A. Laio, and E. Tosatti, Phys. Rev. Lett. **108**, 225701 (2012).